

Distribution of pulmonary ventilation using Xe-enhanced computed tomography in prone and supine dogs

CATHERINE MARCUCCI, DANIEL NYHAN, AND BRETT A. SIMON

*Department of Anesthesia and Critical Care Medicine, Johns Hopkins University
School of Medicine, Baltimore, Maryland 21287-8711*

Received 7 January 2000; accepted in final form 3 August 2000

Marcucci, Catherine, Daniel Nyhan, and Brett A. Simon. Distribution of pulmonary ventilation using Xe-enhanced computed tomography in prone and supine dogs. *J Appl Physiol* 90: 421–430, 2001.—Xe-enhanced computed tomography (CT; Xe-CT) is a method for the noninvasive measurement of regional pulmonary ventilation in intact subjects, determined from the washin and washout rates of the radiodense, nonradioactive gas Xe, as measured in serial CT scans. We used the Xe-CT ventilation method, along with other quantitative CT measurements, to investigate the distribution of regional lung ventilation and air content in healthy, anesthetized, mechanically ventilated dogs in the prone and supine postures. Vertical gradients in regional ventilation and air content were measured in five mongrel dogs in both prone and supine postures at four axial lung locations. In the supine position, ventilation increased with dependent location, with a mean slope of 7.3%/cm lung height, whereas no ventilation gradients were found at any location in the prone position. These results agree quantitatively with other published studies. In addition, six different animals were studied (3 supine, 3 prone) to examine the longitudinal distribution of ventilation and air content. The prone lungs were more uniformly inflated compared with the supine, which were less well expanded at the base than apex. Ventilation index, a measure of regional ventilation relative to whole lung ventilation, increased steeply from apex to base in the supine animals, whereas it was again more uniform in the prone condition. We conclude that the Xe-CT method provides a reasonable, quantitative measurement of regional ventilation and promises to be a valuable tool for the noninvasive determination of regional lung function.

lung volume; lung mechanics; tidal volume; imaging

THE MEASUREMENT OF LUNG VENTILATION, lung volume, and tidal volume (V_T) has traditionally been made for the entire lung, despite the fact that lung function in both health and disease is inhomogeneous. Attempts have been made to quantitate regional lung ventilation both directly and indirectly with a variety of invasive techniques or radioisotope imaging (1, 2, 7, 12, 24, 26, 27, 34, 41, 42), but these methods have been limited by their invasiveness, poor spatial and temporal resolution, qualitative nature, and/or complexity. Xe-enhanced computed tomography (CT; Xe-CT) is a method

for the noninvasive measurement of regional pulmonary ventilation, determined from the washin and washout rates of the radiodense, nonradioactive gas Xe, as measured in serial CT scans. Although the prospect of measuring regional ventilation with stable Xe has been established for many years (17, 18), advances in CT technology have increased the speed and resolution of imaging studies and now make the application of this technique practical for physiological and clinical studies (39). Combined with the unique capability of CT to describe anatomic detail (49) and regional pulmonary perfusion (23), this single imaging modality can potentially provide a nearly complete, noninvasive structural and functional characterization of the lung.

The distributions of ventilation, perfusion, and lung expansion change dramatically between prone and supine body postures, events that have been explored by using a variety of methodologies over many years (1, 21, 26, 33, 40, 47). In fact, these changes are occasionally exploited to improve oxygenation in patients with acute lung injury by placing them into the prone position (15, 28). In this study, we applied the Xe-CT ventilation method and other CT measurements of regional lung function to examine changes in the distribution of ventilation and lung air content in anesthetized dogs in the prone and supine postures, primarily to present and validate the updated Xe-CT method and, in addition, to use these complementary imaging techniques to further explore the physiology of these phenomena.

Xe (atomic no. 54) is a nonradioactive, monatomic noble gas that is denser than air. When imaged in a conventional CT scanner, the density of Xe measured in Hounsfield units (HU) increases linearly with its concentration (Fig. 1). In addition, the degree of CT enhancement depends on the kilovolt setting used, with lower kilovolt settings yielding greater enhancement due to the physical properties of Xe gas. When Xe concentrations of 30–60% in air are delivered to the lung, CT enhancements of parenchymal density of 50–150 HU are obtained. If the Xe is introduced and eliminated from the lung during a controlled washin-

Address for reprint requests and other correspondence: B. A. Simon, Dept. of Anesthesia, Tower 711, Johns Hopkins Hospital, Baltimore, MD 21287-8711 (bsimon@jhmi.edu).

The costs of publication of this article were defrayed in part by the payment of page charges. The article must therefore be hereby marked "advertisement" in accordance with 18 U.S.C. Section 1734 solely to indicate this fact.

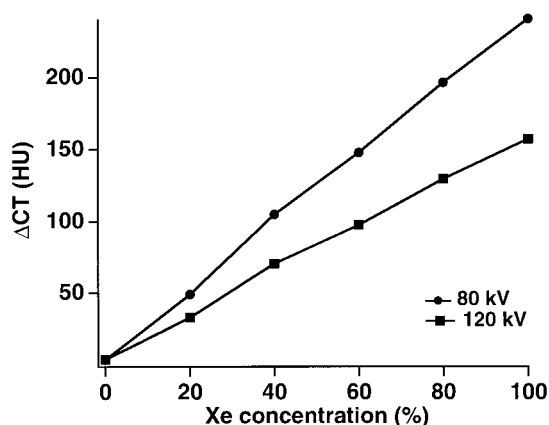


Fig. 1. Xe concentration vs. computed tomography (CT) enhancement [Δ CT; in Hounsfield units (HU)] at 80 and 120 kV. Δ CT measured in a GE9800 CT scanner with Xe gas diluted in air and contained in 60-ml plastic syringes placed within a chest wall phantom.

washout (wi/wo) ventilation protocol, repeat CT scans taken at constant lung volume (i.e., at the same point in the respiratory cycle) will yield a local exponential density curve for any specified region of interest (ROI) within the lung field. The time constant (τ) of this curve is equal to the inverse of the local ventilation per unit volume (specific ventilation, $s\dot{V}$). By selection of different ROI, spatial patterns of ventilation distribution and their changes in response to various interventions can be analyzed. Thus this technique provides the direct, noninvasive measurement of regional ventilation on a scale ranging from $<1 \text{ cm}^3$ volume to the entire lung visible in the CT slice. Furthermore, selecting the ROI over the trachea, through which all gas entering and leaving the lung must pass, allows the calculation of total lung specific ventilation ($s\dot{V}_L$).

In addition to regional ventilation, CT techniques can be used to noninvasively measure many other aspects of lung mechanical function, including the distribution of lung air and tissue volumes (21, 22), the degree of air content of regional lung tissue and recruitment (13, 16, 43), the size of the conducting airways (3, 5), and changes in the configuration of the chest wall and diaphragm (30, 32). By following changes in lung volume and air content at specific anatomical locations as inflation pressure changes, regional mechanical properties may be measured and may provide information complementary to the functional ventilation data of Xe-CT.

METHODS

Experimental preparation. This protocol was approved by the Animal Care and Use Committee of the Johns Hopkins University School of Medicine. Eleven chronic-conditioned male mongrel dogs (20–25 kg) were anesthetized with pentobarbital sodium (25 mg/kg) and fentanyl (15 $\mu\text{g}/\text{kg}$), and relaxed with pancuronium (3 mg) via a forelimb intravenous catheter. The trachea was intubated with a cuffed endotracheal tube (8.0 mm), and the animal was ventilated with a portable piston ventilator (PLV-102, Lifecare International, Westminster, CO) that was modified by the manufacturer to allow remote computer control of all ventilatory parameters.

During the procedure, the animal's oxygen saturation (by Nellcor N-100) and end-tidal carbon dioxide pressure (P_{ETCO_2}) were continuously monitored. Approximately 500–700 ml of Ringer lactate solution was slowly infused over the course of the experiment for maintenance of intravascular volume. At the end of the experimental protocol, residual neuromuscular blockade was reversed with atropine (2–3 mg iv) and neostigmine (2–3 mg iv). All dogs resumed spontaneous ventilation, were extubated, and recovered from anesthesia without incident.

After induction of anesthesia, the animal was carefully positioned on the CT table with gentle forelimb traction. The ventilator was set at 16 respirations/min and 15 ml/kg initial V_T , with the V_T adjusted to maintain a P_{ETCO_2} of 30–32 mmHg. Periodic sighs of three times the V_T were given before each imaging run to minimize atelectasis. A four-channel strip chart recorder was used to record airway pressure, P_{ETCO_2} , airway opening Xe concentration, and a synchronizing signal from the CT scanner. For ventilation studies, Xe was introduced into the breathing circuit by means of a specialized delivery device (Enhancer 3000, Diversified Diagnostic Products, Houston, TX) that meters Xe and O_2 in a closed-circuit system with a CO_2 absorber to provide tight control over the delivered Xe concentration and remote computer-controlled switching between air- O_2 and Xe- O_2 combinations. A Macintosh computer running SuperScope II (GW Instruments, Somerville, MA) was used to automate the experiment by controlling the interface between the CT scanner, the Xe delivery device, and the ventilator, halting the ventilator after each breath to prevent motion artifact during imaging.

Image specifications. All experiments were performed in a GE 9800 CT scanner with settings of 80 kV and 120 mA and were calibrated according to manufacturer's specifications immediately before each experiment. Imaging was performed at the maximum rate of this scanner, resulting in a 2-s scan interval with a 1.2-s prep delay and a 3.6-s interscan delay (net ~ 10 breaths/min during imaging). Image thickness was fixed at 10 mm for all CT scans, with a 512×512 field size and a 22-cm display field of view. Individual images were scaled in real dimensions based on the image field of view size and number of pixels, yielding 0.43 mm/pixel resolution.

Xe-CT ventilation measurement. For measurement of regional ventilation, a series of 40 consecutive end-expiratory CT scans was taken during Xe washin and washout without moving the table position. Two baseline images during 30% O_2 breathing were first obtained, and the inspired gas was switched to 60% Xe-30% O_2 for 18 breaths and then switched back to 30% O_2 for the 20-breath washout period. After baseline conditions were reestablished, the table was moved to the next location and the process was repeated.

Protocols. In *protocol 1*, regional ventilation was determined in five animals, in both the prone and supine positions, at four discrete anatomic locations: midapex (apex), carina, mid-lower lung (midbase), and lung base (Fig. 2). The table locations at these positions were selected from a functional residual capacity (FRC) whole lung image series, with care taken not to move the dog after this initial scanning. Discrete anatomic structures in the lung fields (blood vessels, bronchi) were noted and matched when turning the animal prone so that the same approximate longitudinal lung location was imaged in both the prone and supine positions. These data were used to compare the vertical distribution of lung air content and regional ventilation in the same animals when changing posture. A second protocol (*protocol 2*) was performed to determine the longitudinal (apex to base) distribution of ventilation with greater spatial resolution. In six dogs

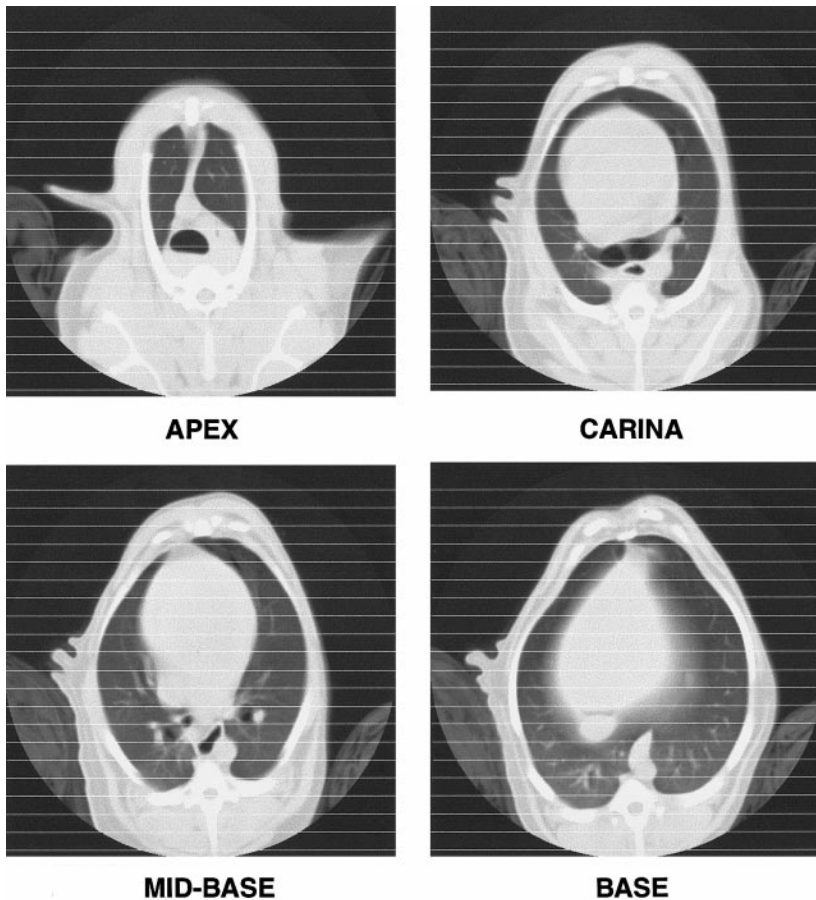


Fig. 2. CT image locations for *protocol 1*.

(3 prone, 3 supine), Xe-CT ventilation was measured in every other 10-mm-thick slice from apex to base, resulting in 9–12 measurements per dog. Because of the time required for these experiments, it was not possible to study the same dogs prone and supine in one sitting. These data were analyzed in terms of average ventilation of the left and right lungs within each slice, plotted as a function of their longitudinal position.

Image analysis. The images were archived and transferred over the hospital network to a Macintosh computer, which was used for all subsequent analysis. Quantitative image analysis was performed using NIH Image (a public-domain software package available on the Internet from <http://rsb.info.nih.gov/nih-image/>). This powerful program has a variety of flexible analytical tools and programming capability that allows the efficient automation of complex, multistep image analyses. The 16-bit CT images were windowed and scaled to 8-bit, with a density resolution of 5 HU. For convenience, the units of density used are HU offset by 1,000 (HU + 1,000), so that air has a density of 0 and water 1,000 (instead of -1,000 and 0, respectively, as with standard HU). The lung tissue within a given slice is outlined with use of a thresholding function, which separates lung tissue from the surrounding structures by density range. Further subdivision of the lung into smaller ROI for regional analysis may then be performed as required.

For analysis of lung volume and air content distribution, images are first calibrated in terms of percent air content by assuming that each voxel is made up of a linear combination of air and tissue, each with a known density determined from measurements made over the heart and trachea. The air volume contained in each slice is then calculated from the

product of slice lung volume (thresholded area \times image thickness) and average percent air content. The sum of the air volumes of all the slices is equal to the total lung air volume. The trachea and mainstem bronchi are excluded from this analysis. Within a slice, the vertical distribution of air content was analyzed by dividing the lung into 1-cm-high horizontal ROI (Fig. 2) and plotting the percent air of each segment against vertical position.

For analysis of Xe-CT images, the mean density in each ROI was measured in each image in the series and then plotted as a function of time (Fig. 3). τ Was determined by

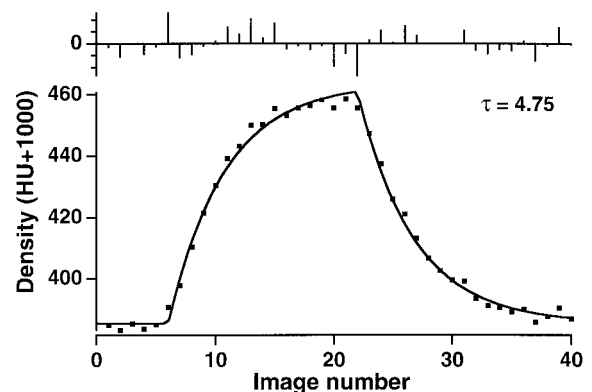


Fig. 3. Example density-time curve for a lung region of interest during Xe gas washin-washout study. τ , Time constant. Graph at *top* shows curve-fit residuals.

fitting this curve to a single-compartment exponential model using a nonlinear least squares curve-fitting procedure (Igor Pro, WaveMetrics, Lake Oswego, OR). τ is constrained to be the same for the washin and washout portions of the curve (36). The starting points of the washin and/or washout segments (t_0 and t_1) are initially estimated by visual inspection of the curves and then determined by the curve-fitting procedure. Although imaging occurs once per breath, t_0 and t_1 are permitted to take on fractional values, reflecting that the arrival of Xe to the lung periphery may occur in midcycle because of the variable amount of dead space relative to V_T in the system and down a given pathway. Goodness of fit was assessed by examination of the normalized summed squared residuals of the data, and 95% confidence intervals for τ were estimated by using a Monte Carlo method that has previously been described and validated (36). Because images are obtained once per breath, τ is conveniently given in units of breaths, which may be converted to time units by dividing by the respiratory frequency. To normalize for differences in absolute ventilation between dogs, some ventilation data are presented as ventilation index (VI), defined as the regional $s\dot{V}/s\dot{V}_L$, where $s\dot{V}_L$ is estimated from a ROI placed within the trachea. A VI of 1 indicates that the region is being ventilated at a rate equal to that of the whole lung.

Statistical analysis. Data are presented as means \pm SE unless otherwise noted. Differences between means were tested by paired *t*-tests (Statview 4.5, Abacus Concepts, Berkeley, CA) with a significance level of $P < 0.05$.

RESULTS

Longitudinal volume profile. A plot of the typical distribution of lung volume at FRC from apex to base in supine and prone postures is presented in Fig. 4 (top). In the prone position, the diaphragm assumes a flatter profile, resulting in a smaller maximum cross-sectional area and a longer axial extent. Lung volume at FRC, determined by summing the air volumes of all the individual slices, was not significantly different in the supine vs. prone position (supine-to-prone FRC volume ratio $95.4 \pm 3.4\%$, $P = 0.21$). The distribution of air content (%air) for each slice is depicted in Fig. 4 (bottom). Note that, in the supine position, the apex is well expanded, whereas there is compression of the lung base under the diaphragm compared with the relatively uniform expansion seen in the prone position. The approximate position of the four imaging planes in protocol 1 are indicated in the figure.

Gravitational ventilation gradients. A graph of VI vs. vertical height shows a gravity-dependent gradient in ventilation, with ventilation greatest in the most dependent regions, at all four locations in the supine but not the prone dog (Fig. 5). Straight lines were fitted to these individual left and right lung VI-vs.-height data for each animal to determine average slopes or gradients (Table 1). There were no significant differences in slope between any individual locations within the supine or prone animals. However, the mean slope of all the supine lungs of -0.073 ± 0.007 (mean \pm SE) was significantly steeper than the slope of -0.008 ± 0.009 of the prone lungs ($P < 0.0001$), indicating a mean ventilation gradient of $\sim 7\%$ of the total $s\dot{V}$ per centimeter lung height in the supine position, with $s\dot{V}$ greatest in the most dependent regions. The slopes in

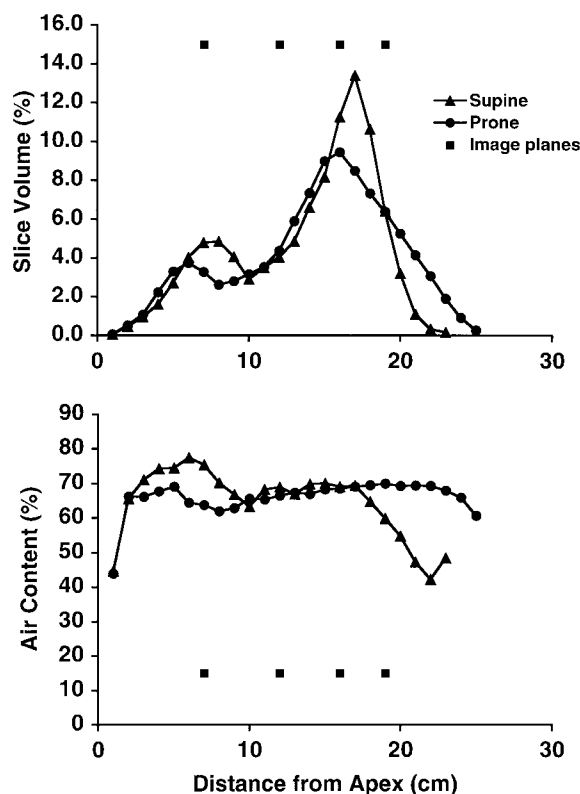


Fig. 4. Apex-to-base distribution of air volume (top; expressed as % of total) and average air content (bottom) for a representative dog at functional residual capacity. Squares indicate location of the imaging planes from Fig. 3.

the prone position were not significantly different from zero ($P = 0.37$).

The contribution of the vertical ventilation gradients to overall ventilation variability was estimated by stepwise multiple linear regression, using VI as the dependent variable and height (*Y*), side (*S*, left vs. right), and longitudinal location (*Z*, apex-base) as independent variables. The means and standard deviation of R^2 for the five animals are presented in Table 2. In the supine position, the vertical gradient accounted for $37 \pm 7\%$ of the variance ($P < 0.01$), with less than an additional 4% explained by the addition of *S* and *Z*. In the prone position, all variables accounted for only 5–7% of the variance (not significant).

Gravitational air content gradients. Strong gravitational gradients in FRC lung air content were also seen in the supine position at all imaging planes, with air content increasing from dependent to nondependent ROI. In the prone position, however, the gradient changed with location, being negative at the apex (opposite that in the supine position), flat at the carina, and then slightly positive at the midbase and base. Note that these gradients are expressed in terms of the gravitational or vertical coordinate rather than the animal's anatomic dorsal-ventral position. Thus reversal of the gravitational air content gradient at the apex means that the dorsal lung regions were least expanded in both supine and prone positions. In the prone position, the air content gradient went against

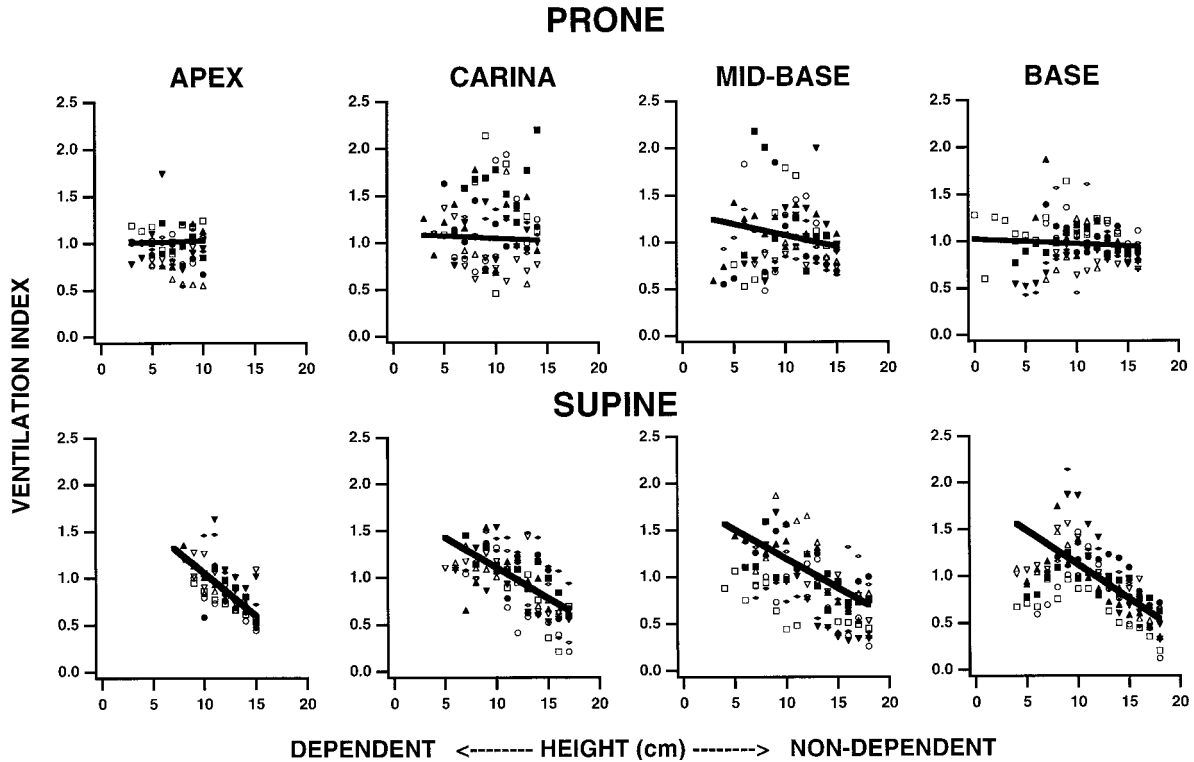


Fig. 5. Ventilation index (VI) vs. region of interest height for 5 dogs in prone and supine positions at different imaging locations. Symbols are individual left and right lungs. Heavy lines are means of linear regressions, calculated separately for each lung.

gravity at the apex, was uniform at the carina, and went with gravity at the midbase and base. Straight lines were fitted to the data, and the resulting slopes are presented in Table 1. There were no differences between left and right lungs at any location. In the supine dogs, the slope at the apex was significantly steeper than at the other three locations ($P < 0.01$), which were not different from each other ($P > 0.11$). In the prone position, the slopes at the apex and carina differed from each other ($P = 0.03$) and from the midbase and base ($P < 0.03$), which did not significantly differ from each other ($P > 0.28$). The slopes of the VI and %air gradients were weakly correlated in the supine position ($r = -0.32$, $P = 0.046$) and not correlated in the prone position ($r = -0.11$, $P = 0.51$). Average air content for the entire lung was $66.8 \pm 1.7\%$ supine and $67.3 \pm 2.1\%$ prone.

Longitudinal ventilation distribution. The distribution of ventilation from apex to base in three supine and three prone dogs is presented (Fig. 6) as both VI, which gives the slice \dot{V} normalized to the whole lung \dot{V} , and as slice ventilation (%), which is the net slice ventilation expressed as percentage of total measured lung ventilation (sum of all slice ventilations). The VI gives the relative ventilation of a region compared with that of the lung as a whole. The slice ventilation (%) gives the fractional contribution of that region to the total lung ventilation. Because the net slice ventilation is obtained by multiplying the slice \dot{V} by the total volume of the slice, its distribution is strongly influenced by the different FRC volume distribution profiles (Fig. 4). In the supine position, \dot{V} steadily increases from apex to base (Fig. 6). Coupled with the volume profile of the supine lung (Fig. 4), this results in an

Table 1. Slopes of VI and %air vs. height

	Supine		Prone	
	Slope of VI vs. Height, cm^{-1}	Slope of %Air vs. Height, %air/cm	Slope of VI vs. Height, cm^{-1}	Slope of %Air vs. Height, %air/cm
Apex	-0.091 ± 0.013	3.474 ± 0.356	0.004 ± 0.018	-1.390 ± 0.341
Carina	-0.065 ± 0.008	2.466 ± 0.353	-0.005 ± 0.020	0.213 ± 0.338
Midbase	-0.062 ± 0.010	2.110 ± 0.182	-0.024 ± 0.023	1.015 ± 0.243
Base	-0.073 ± 0.021	2.246 ± 0.182	-0.005 ± 0.009	1.233 ± 0.275
All	-0.073 ± 0.007	2.574 ± 0.156	-0.008 ± 0.009	0.268 ± 0.218

Values are means \pm SE, $n = 10$ (5 dogs, left and right lungs analyzed separately). VI, ventilation index; %air, distribution of air content.

Table 2. Stepwise multiple regression of VI vs. position

	Supine
Y	0.369 ± 0.07
Y/S	0.376 ± 0.07
Y/Z	0.404 ± 0.07
Y/S/Z	0.410 ± 0.06
	Prone
Y	0.049 ± 0.05
Y/S	0.054 ± 0.05
Y/Z	0.065 ± 0.05
Y/S/Z	0.070 ± 0.05

Values are means ± SD for R^2 ; $n = 5$ dogs. Y, height; S, side (left vs. right); Z, longitudinal location (apex-base).

even steeper distribution of slice ventilation moving toward the base (Fig. 6). On the other hand, the distribution of sV in the prone animals is flat or decreases toward the lung base (Fig. 6). Because the longitudinal distribution of prone lung volume is more uniform (Fig. 4), this causes a comparatively more even distribution of slice ventilation that reaches a maximum between the carina and lung base (Fig. 6).

DISCUSSION

The use of imaging technology is supplanting, in many cases, more traditional physiological studies because of the need for noninvasive determination of regional structure and function in intact organisms. Although many technologies are available, X-ray CT is emerging as the preferred modality for imaging of the lung because of its widespread availability, resolution, high signal-to-noise ratio for lung tissue, and speed. Technology is advancing rapidly, and scanners are readily available that can perform high-resolution scans of an entire human lung in <30 s. In addition to its traditional role in identifying abnormal lung anatomy or pathological lesions, CT has been used to image changes in airway dimensions in studies of re-

active airway diseases (4) and volume overload (6) and to describe changes that occur in chest wall and diaphragm configuration with position, anesthesia, pleural effusion, and lung resection (9, 30, 32). The bronchial and vascular trees have been extracted and reconstructed in three dimensions from high-resolution images (46), and CT techniques have been developed to measure regional pulmonary perfusion (23). CT measurements of the regional distribution of lung density/inflation in patients with acute respiratory distress syndrome, and how these parameters change with positive end-expiratory pressure and body position, have provided crucial insight into ventilator management of these critically ill patients (14, 33). The addition of the Xe-CT technique for measuring regional ventilation to these previously available methodologies makes possible the use of CT imaging to create a nearly complete anatomic and quantitative functional characterization of the lung.

Xe is a stable, nonradioactive, inert gas that is weakly radiodense (Fig. 1), making it useful as a radiographic contrast agent for highly sensitive imaging modalities such as CT but not plain radiographs or fluoroscopy (35, 45). It is relatively insoluble [blood-gas partition coefficient 0.14 (38)], but adequate radiodensity is transferred from the lung to the blood and tissues to make measurement of cerebral blood flow possible (11). This technique was extended to the measurement of local pulmonary ventilation in animals (17, 18) and in healthy and critically ill humans (20, 37) over 20 years ago. Although Xe is an inert gas, it is also an inhaled anesthetic (minimum alveolar concentration 71%), ~30% more potent than nitrous oxide (8) and in clinical use in many countries (10). A large number of human volunteers and patients have inhaled 30–50% Xe for cerebral blood flow studies with an excellent safety record, although sedating or other anesthetic side effects increase with concentrations above 35% (19, 48). Finally, Xe is a relatively expensive gas (10, 31), making a device such as the Enhancer

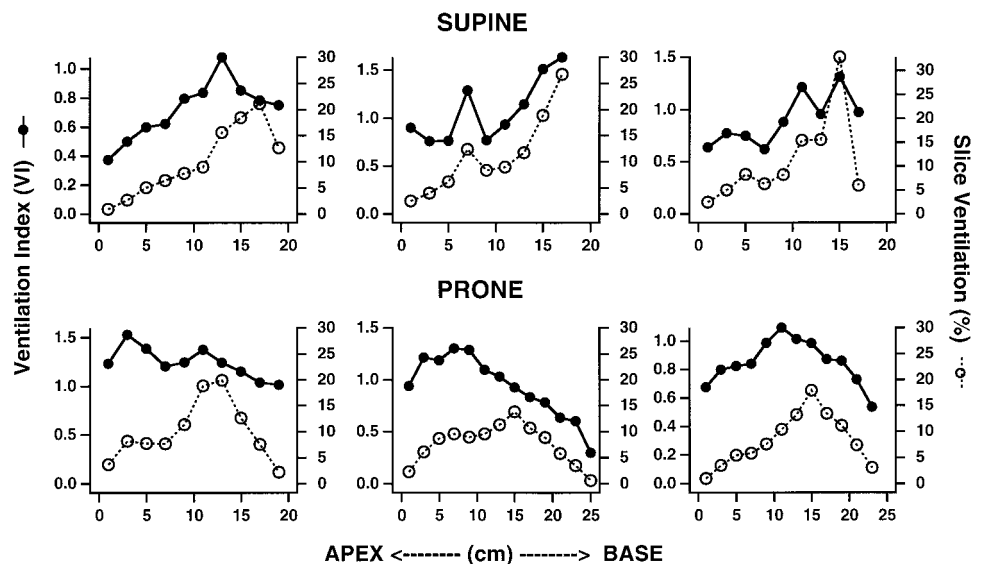


Fig. 6. Apex-to-base distributions of VI (●) and slice ventilation (○, expressed as % of total lung ventilation) in 3 prone and 3 supine dogs.

3000, which allows rebreathing of Xe in a closed circuit while absorbing CO₂ and regulating the inspired Xe and O₂ concentrations, essential for the economical application of this technique.

Methodological considerations. The Xe-CT technique described here for measurement of pulmonary ventilation is a variation of the familiar indicator-dilution method. However, unlike radioactive tracer methods, in which essentially all the radioactive counts measured are introduced by the tracer, changes in density measured in the serial CT scans must be distinguished between those resulting from increasing concentration of the tracer gas vs. changes in the underlying substrate (i.e., lung) density. Lung density will change with small changes in lung volume, misregistration of the identical ROI from image to image, and changes in blood volume within the ROI. The changes in lung density that occur with a single inspiration are greater than the 50–80 HU enhancement typically seen with 60% Xe equilibration, and thus it is critical that each image be obtained at the same lung volume. In studies of mechanically ventilated animals, this is most easily done at end-expiration; end-inspiratory holds are potentially complicated by stress relaxation or creep. Changes in background or lung density account for the majority of the noise in estimating the regional time constants, and this noise, rather than the spatial resolution of the CT scanner, is what ultimately limits the spatial resolution of the measurement (36). For example, because cardiac motion contributes to this noise to a varying degree depending on the distance to the heart, the actual spatial resolution realized may vary with location, as indicated by the width of the confidence interval about a calculated τ or $s\dot{V}$ value (36). Cardiac gating using an ultrafast CT scanner has been shown to greatly reduce this particular source of noise (39). Using relatively thick slices (5–10 mm vs. 0.5–1.5 mm for high-resolution CT) can reduce noise by averaging density over a larger volume, reducing partial volume effects for small registration errors but at the expense of increasing partial volume effects at the lung boundary and reducing spatial resolution. In these animal studies, 60% Xe was used to maximize the density-enhancement signal and thereby minimize these noise effects. For human studies, a lower Xe concentration will be required to limit anesthetic side effects, making the use of cardiac gating and other methods to minimize error even more important.

A wi/wo experimental protocol was used because, in a previously published model simulation (36), we showed that, given the same nominal parameters, noise level, and number of images, the wi/wo model yields better τ estimates than either a washin or washout protocol alone. This occurs because most of the information in estimating an exponential is contained in the steep initial portion of the curve, and the wi/wo model has two such segments compared with only one for the washin and washout models. To maximize the data available for parameter estimation, we imaged the lung every breath during the protocol, because there was no concern about cumulative radiation expo-

sure for these studies. For application of this method to humans, however, it is likely that an optimized imaging protocol that acquires images more frequently during the early, rapidly changing portion of the washin and washout phases would be more appropriate. Furthermore, a single-compartment model was used. This appears to be adequate for the healthy lung, but more complex, multicompartment models may be required in injured lungs. However, if the ROI used is relatively small, it is likely that single-compartment behavior may still be approximated, even in an abnormal lung.

Absolute values of $s\dot{V}$ will vary among animals, ventilator settings, and different experimental conditions. To facilitate comparisons and to examine changes in the distribution of ventilation, the VI was used, in which regional $s\dot{V}$ was normalized by whole lung $s\dot{V}$. Whole lung ventilation was estimated from the wi/wo curve of a ROI placed within the trachea. If the whole lung ventilation is over- or underestimated, as might occur if there is significant regional heterogeneity such that the whole lung washout departs from the single exponential model, then all the VI for that study will be biased. This may account for why some of the VI data in Fig. 6 do not appear to have a mean VI of 1. However, even if biased, the VI parameter remains useful for looking at changes in the distribution of ventilation within an animal.

The Xe-CT ventilation method requires a large number of serial scans to be taken at each imaging location, typically 40–50 breaths or 4–6 min per study. Lung regions with very long time constants and low ventilatory rates will require longer washin and washout times, although total equilibration is not necessary to obtain accurate regional time constants. On the other hand, these studies are performed without interrupting ventilation and thus give an accurate reflection of steady-state ventilatory conditions. The CT technology used in this study required repeating the full imaging protocol at each location, limiting the number of locations and/or conditions that could be studied because of time constraints. More modern CT scanners are already available that are capable of high-speed volumetric image acquisition, allowing the simultaneous acquisition of multiple imaging planes.

Vertical gradients of ventilation and air content. In agreement with the literature, important differences in the distribution of regional ventilation between the prone and supine postures were found (Table 1). In the supine posture, there was a steep gradient in $s\dot{V}$, with increased ventilation in the more dependent regions. In contrast, no gradient in ventilation was found in the prone position. Many other studies using a variety of techniques have shown similar patterns of ventilation. The slope of VI vs. height for the supine lungs (all locations combined) was $-0.073 \pm 0.007 \text{ cm}^{-1}$ (mean \pm SE) or 7.3%/cm, which is remarkably close to the value of -0.069 ± 0.015 determined by Hubmayr et al. (26) following the volumes of groups of implanted marker with biplane X-ray cine during stepwise deflation from total lung capacity in supine dogs. In another study using implanted markers in mechanically ventilated

dogs, these authors measured the vertical gradient in regional V_T/FRC (25), a parameter comparable to our $s\dot{V}$. They found mean gradients of 0.005 and -0.032 cm^{-1} in prone and supine postures, respectively, compared with -0.002 and -0.014 cm^{-1} in our study. Using aerosolized fluorescent microspheres, Robertson et al. (34) found no significant vertical ventilation gradients in prone pigs. Treppo et al. (40) used radioactive $N-^{13}N$ positron emission tomography imaging to simultaneously measure ventilation, perfusion, alveolar volume, and \dot{V}/Q at the lung base in dogs and found a gradient in $s\dot{V}$ of $5.52 \pm 1.1\%/cm$ (mean \pm SD) in the supine position vs. $0.34 \pm 0.88\%/cm$ when dogs were turned prone. Our results agree quantitatively with these diverse studies, both reiterating this important change in regional lung function with posture and validating the Xe-CT technique.

The vertical gradient in ventilation in the supine posture accounted for 37% of the total variance in VI distribution, determined from the R^2 values of stepwise multiple regression analysis, with little additional contribution from left vs. right side or craniocaudal location. No significant contribution of position was found for the prone posture. These data were obtained by using 1-cm-high horizontal ROIs, rather than uniformly or randomly oriented ROIs. This sampling approach could possibly have biased the analysis toward attributing a radial or hilar-to-peripheral ventilation gradient to the vertical coordinate. However, Hubmayr et al. (26), fitting both vertical and craniocaudal position data to ventilation distribution, found R^2 values of 0.39 for the upper lobes, 0.34 for the lower lobes, and an average of 0.37 for the entire lung in supine dogs. Treppo et al. (40) found that the vertical gradient accounted for 33.2% of total variance in ventilation in supine dogs, with no significant contribution of vertical position in the prone position. The close agreement of our results with those of these prior studies suggests that the use of horizontal ROIs did not significantly bias our result.

Vertical patterns of air content also differed with posture, although the pattern did not closely follow the distribution of ventilation as might have been expected if one assumed that the air content was inversely proportional to the local elastance. In the supine position, there was a consistent gradient in lung expansion, least expanded in the dependent regions and significantly steeper at the apex than at the other locations (Table 1). The ventilation gradients took a similar form, although the steeper slope also seen at the apex was not statistically significant. In the prone position, the air content gradient changed with location such that it exhibited an inverse relationship to gravity at the apex, was uniform at the carina, and then reestablished a gravitational gradient toward the base, which was about half as steep as at that location in the supine position. The prone ventilation gradients, however, were not different from zero at any location. To evaluate whether the lung locations with the steepest air content gradients also had the steepest ventilation gradients, standard correlation coefficients were calculated (Statview 4.5, Abacus Concepts, Berkeley, CA).

The vertical gradients in air content and ventilation were only weakly correlated in the supine position ($R = 0.32$, $P = 0.046$), and not at all in the prone position ($R = 0.11$, $P = 0.51$), and these correlations were not improved by looking at regional subsets of the data.

Hoffman (21) used the dynamic spatial reconstructor to study regional lung expansion in anesthetized dogs and found an average vertical gradient of air content at FRC of 3.3%air/cm supine and -0.36% air/cm prone. These values compare well to the 2.57 ± 0.16 and $0.27 \pm 0.22\%$ air/cm gradients found in our supine and prone dogs, respectively (Table 1). Although these studies analyzed the entire lung, they measured the gradient from the average air content of coronal slices running from apex to base and thus did not examine regional differences in vertical gradients. The average air content described by these authors in the prone position, 66%, also agrees well with the $67.3 \pm 2.1\%$ prone and $66.8 \pm 1.7\%$ supine measured in our animals. Other studies looking at postural gradients of pleural pressure (44), subpleural alveolar size (47), and positron emission tomography measurement of alveolar volume (40) have similarly found steep gradients in the supine position and minimal or no gradients when prone.

Longitudinal distributions of ventilation and volume. The apex-to-base distribution of lung volume consistently changes with posture (Fig. 4), as has been previously described by others (22, 23, 30), such that the profile of the prone lung is flatter. The region below the heart is more compressed and the diaphragm is steeper due to pressure from the abdominal contents in the supine position, resulting in compression of the dependent lung and distortion of the chest wall, which combine to create the strong gradients in regional pleural pressure and lung expansion noted above (29, 30).

VI, which describes the regional $s\dot{V}$ relative to that of the whole lung, increases in the supine posture from apex to base (Fig. 5). This increase must reflect the fact that the lung base and diaphragm, which are compressed by the abdominal contents at FRC (Fig. 4), are initially more compliant than the apex and midlung. In fact, relatively little radial expansion of the apical chest wall occurs, even with inflation to total lung capacity (21, 30). As the lung expands, it moves caudally and displaces the diaphragm; in the supine dogs, the abdominal contents are resting on the basal lung, and their displacement apparently presents less impedance to lung expansion than does the more rigid chest wall. The less expanded basal lung tissue may also be more compliant, further contributing to the higher $s\dot{V}$ of this region. Combining this pattern of $s\dot{V}$ with the steeper profile of lung volume toward the base further accentuates the apex-base increase in slice ventilation in the supine position (Fig. 5). In contrast, in the prone position, the heart and abdominal contents fall away from the lung, the lung at FRC is very uniformly inflated (Fig. 4), and the longitudinal distribution of $s\dot{V}$ is likewise relatively uniform. Combined with the lung volume profile, the net result for the prone condition is a more even distribution of slice

ventilation that reaches a maximum below the carina and falls off toward the base.

The prone position has been shown to dramatically improve oxygenation in a subset of patients with acute lung injury, a result of the reduction in the vertical pleural pressure gradient and improved recruitment of dependent lung regions (15, 28). Although the above findings in healthy animals need to be repeated in models of lung injury, they highlight the importance of postural changes in the distribution of lung expansion and ventilation, which are thought to be critical factors contributing to this phenomenon. Indeed, although much attention has been focused on the changing vertical gradient in ventilation with the prone position, it is entirely possible that the longitudinal differences in air content and ventilation are of equal or greater importance.

Summary. CT imaging provides noninvasive information on lung structure and function that permits the extension of studies of lung mechanics and physiology from the whole organ to the regional level. The Xe-CT ventilation method adds to this armamentarium, providing a quantitative measure of regional pulmonary ventilation to complement the data on regional lung volumes and air content traditionally obtained from CT studies. Results of these Xe-CT studies of healthy animals in the prone and supine postures demonstrate significant regional nonuniformities and agree with findings from the literature and with commonly accepted concepts of regional lung mechanical function.

We thank Dr. Wayne Mitzner for invaluable advice and encouragement, Dr. Elias Zerhouni for access to the CT imaging facilities, Vince Lerie for expert CT technological support, and especially Mansheung Fung for work developing the software for controlling the ventilator and Xe delivery system. We are indebted to Praxair Pharmaceuticals, Tarrytown, NY, for providing the Xe gas, Jerry Timpe of Diversified Diagnostic Products, Houston, TX, for providing the Enhancer 3000 Xe delivery system, and Lifecare International, Westminster, CO, for providing the computer-controlled PLV-102 ventilator.

This research was supported by National Heart, Lung, and Blood Institute Grant HL-58504 and American Heart Association Grant MDBG0495.

REFERENCES

1. Ball WC, Stewart PB, Newsham LGS, and Bates DV. Regional pulmonary function studied with xenon¹³³. *J Clin Invest* 41: 519–531, 1962.
2. Berdine GG, Lehr JL, McKinley DS, and Drazen JM. Non-uniformity of canine lung washout by high-frequency ventilation. *J Appl Physiol* 61: 1388–1394, 1986.
3. Brown RH, Herold CJ, Hirshman CA, Zerhouni EA, and Mitzner W. In vivo measurements of airway reactivity using high-resolution computed tomography. *Am Rev Respir Dis* 144: 208–212, 1991.
4. Brown RH, Herold CJ, Hirshman CA, Zerhouni EA, and Mitzner W. Individual airway constrictor response heterogeneity to histamine assessed by high-resolution computed tomography. *J Appl Physiol* 74: 2615–2620, 1993.
5. Brown RH, Zerhouni EA, and Hirshman CA. Reversal of bronchoconstriction by inhaled nitric oxide: histamine versus methacholine. *Am J Respir Crit Care Med* 150: 233–237, 1994.
6. Brown RH, Zerhouni EA, and Mitzner W. Visualization of airway obstruction in vivo during lung vascular engorgement and edema. *J Appl Physiol* 78: 1070–1078, 1995.
7. Bunow B, Line BR, Horton MR, and Weiss GH. Regional ventilatory clearance by xenon scintigraphy: a critical evaluation of two estimation procedures. *J Nucl Med* 20: 703–710, 1979.
8. Cullen SC, Eger EI, Cullen BF, and Gregory P. Observations on the anesthetic effect of the combination of xenon and halothane. *Anesthesiology* 31: 305–309, 1969.
9. Dechman G, Mishima M, and Bates JHT. Assessment of acute pleural effusion in dogs by computed tomography. *J Appl Physiol* 76: 1993–1998, 1994.
10. Dingley J, Ivanova-Stoilova TM, Grundler S, and Wall T. Xenon: recent developments. *Anaesthesia* 54: 335–346, 1999.
11. Drayer BP, Sidney W, and Reinmuth OM. Xenon enhanced CT for analysis of cerebral integrity, perfusion, and blood flow. *Stroke* 9: 123–130, 1978.
12. Fredberg JJ, Keefe DH, Glass GM, Castile RG, and Frantz ID III. Alveolar pressure nonhomogeneity during small-amplitude high-frequency oscillation. *J Appl Physiol* 57: 788–800, 1984.
13. Gattinoni L, D'Andrea L, Pelosi P, Vitale G, Pesenti A, and Fumagalli R. Regional effects and mechanism of positive end-expiratory pressure in early adult respiratory distress syndrome. *JAMA* 269: 2122–2127, 1993.
14. Gattinoni L, Pelosi P, Pesenti A, Brazzi L, Vitale G, Morletto A, Crespi A, and Tagliabue M. CT scan in ARDS: clinical and physiopathological insights. *Acta Anaesthesiol Scand* 95: 87–96, 1991.
15. Gattinoni L, Pelosi P, Vitale G, Pesenti A, D'Andrea L, and Mascheroni D. Body position changes redistribute lung computed-tomographic density in patients with acute respiratory failure. *Anesthesiology* 74: 15–23, 1991.
16. Gattinoni L, Pesenti A, Bombino M, Baglioni S, Rivolta M, Rossi F, Rossi G, Fumagalli R, Marcolin R, Mascheroni D, and Torresin A. Relationships between lung computed tomographic density, gas exchange, and PEEP in acute respiratory failure. *Anesthesiology* 69: 824–832, 1988.
17. Gur D, Drayer BP, Borovetz HS, Griffith BP, Hardesty RL, and Wolfson SK. Dynamic computed tomography of the lung: regional ventilation measurements. *J Comput Assist Tomogr* 3: 749–753, 1979.
18. Gur D, Shabason L, Borovetz HS, Herbert DL, Reece GJ, Kennedy WH, and Serago C. Regional pulmonary ventilation measurements by xenon enhanced dynamic computed tomography: an update. *J Comput Assist Tomogr* 5: 678–683, 1981.
19. Haughton VM, Donegan JH, Walsh PR, Syvertsen A, and Williams AL. A clinical evaluation of xenon enhancement for computed tomography. *Invest Radiol* 15: 160–163, 1980.
20. Herbert DL, Gur D, Shabason L, Good WF, Rinaldo JE, Snyder JV, Borovetz HS, and Mancini MC. Mapping of human local pulmonary ventilation by xenon enhanced computed tomography. *J Comput Assist Tomogr* 6: 1088–1093, 1982.
21. Hoffman EA. Effect of body orientation on regional lung expansion: a computed tomographic approach. *J Appl Physiol* 59: 468–480, 1985.
22. Hoffman EA and Ritman EL. Effect of body orientation on regional lung expansion in dog and sloth. *J Appl Physiol* 59: 481–491, 1985.
23. Hoffman EA, Tajik JK, and Kugelmass SD. Matching pulmonary structure and perfusion via combined dynamic multislice CT and thin-slice high-resolution CT. *Comput Med Imaging Graph* 19: 101–112, 1995.
24. Hubmayr RD, Hill MJ, and Wilson TA. Nonuniform expansion of constricted dog lungs. *J Appl Physiol* 80: 522–530, 1996.
25. Hubmayr RD, Rodarte JR, Walters BJ, and Tonelli FM. Regional ventilation during spontaneous breathing and mechanical ventilation in dogs. *J Appl Physiol* 63: 2467–2475, 1987.
26. Hubmayr RD, Walters BJ, Chevalier PA, Rodarte JR, and Olson LE. Topographical distribution of regional lung volume in anesthetized dogs. *J Appl Physiol* 54: 1048–1056, 1983.
27. Jones RL, Overton TR, and Sproule BJ. Frequency dependence of ventilation distribution in normal and obstructed lungs. *J Appl Physiol* 42: 548–553, 1977.
28. Lamm WJ, Graham MM, and Albert RK. Mechanism by which the prone position improves oxygenation in acute lung injury. *Am J Respir Crit Care Med* 150: 184–193, 1994.

29. **Liu S, Margulies SS, and Wilson TA.** Deformation of the dog lung in the chest wall. *J Appl Physiol* 68: 1979–1987, 1990.
30. **Margulies SS and Rodarte JR.** Shape of the chest wall in the prone and supine anesthetized dog. *J Appl Physiol* 68: 1970–1978, 1990.
31. **Nakata Y, Goto T, Niimi Y, and Morita S.** Cost analysis of xenon anesthesia: a comparison with nitrous oxide-isoflurane and nitrous oxide-sevoflurane anesthesia. *J Clin Anesth* 11: 477–481, 1999.
32. **Olson LE and Hoffman EA.** Lung volumes and distribution of regional air content determined by cine X-ray CT of pneumonectomized rabbits. *J Appl Physiol* 76: 1774–1785, 1994.
33. **Pelosi P, D'Andrea L, Vitale G, Pesenti A, and Gattinoni L.** Vertical gradient of regional lung inflation in adult respiratory distress syndrome. *Am J Respir Crit Care Med* 149: 8–13, 1994.
34. **Robertson HT, Glenny RW, Stanford D, McInnes LM, Luchtel LD, and Covert D.** High-resolution maps of regional ventilation utilizing inhaled fluorescent microspheres. *J Appl Physiol* 82: 943–953, 1997.
35. **Rockoff SD and Mendelsohn ML.** Evaluation of xenon as a gaseous roentgenographic contrast material. *Am Rev Respir Dis* 86: 434–438, 1962.
36. **Simon BA, Marcucci C, Fung M, and Lele SR.** Parameter estimation and confidence intervals for Xe-CT ventilation studies: a Monte Carlo approach. *J Appl Physiol* 84: 709–716, 1998.
37. **Snyder JV, Pennock B, Herbert DL, Rinaldo JE, Culpepper J, Good WF, and Gur D.** Local lung ventilation in critically ill patients using nonradioactive xenon-enhanced transmission computed tomography. *Crit Care Med* 12: 46–51, 1984.
38. **Steward A, Allott PR, Cowles AL, and Mapleson WW.** Solubility coefficients for inhaled anesthetics for water, oil, and biological media. *Br J Anaesth* 45: 282–293, 1973.
39. **Tajik JK, Tran BQ, and Hoffman EA.** Xenon enhanced CT imaging of local pulmonary ventilation. *Proc SPIE* 2709: 40–54, 1996.
40. **Treppo S, Mijailovich SM, and Venegas JG.** Contributions of pulmonary perfusion and ventilation to heterogeneity in \dot{V}/\dot{Q} measured by PET. *J Appl Physiol* 82: 1163–1176, 1997.
41. **Van der Mark TW, Rookmaker AEC, Kiers A, Peset R, Vaalburg W, Paans AMJ, and Woldring MG.** Nitrogen-13 and xenon-133 ventilation studies. *J Nucl Med* 25: 1175–1182, 1984.
42. **Venegas JG, Yamada Y, Custer J, and Hales CA.** Effects of respiratory variables on regional gas transport during high-frequency ventilation. *J Appl Physiol* 64: 2108–2118, 1988.
43. **Vieira SRR, Puybasset L, Lu Q, Richecoeur J, Cluzel P, Coriat P, and Rouby J.** A scanographic assessment of pulmonary morphology in acute lung injury. *Am J Respir Crit Care Med* 159: 1612–1623, 1999.
44. **Wiener-Kronish JP, Gropper MA, and Lai-Fook SJ.** Pleural liquid pressure in dogs measured using a rib capsule. *J Appl Physiol* 59: 597–602, 1985.
45. **Winkler SS, Holden JE, Sackett JF, Flemming DC, and Alexander SC.** Xenon and krypton as radiographic inhalation contrast media with computerized tomography: preliminary note. *Invest Radiol* 12: 19–20, 1977.
46. **Wood SA, Zerhouni EA, Hoford JD, Hoffman EA, and Mitzner W.** Measurement of three-dimensional lung tree structures by using computed tomography. *J Appl Physiol* 79: 1687–1697, 1995.
47. **Yang Q, Kaplowitz MR, and Lai-Fook SJ.** Regional variations in lung expansion in rabbits: prone vs. supine positions. *J Appl Physiol* 67: 1371–1376, 1989.
48. **Yonas H, Grundy B, Gur D, Shabason L, Wolfson SK Jr, and Cook EE.** Side effects of xenon inhalation. *J Comput Assist Tomogr* 5: 591–592, 1981.
49. **Zerhouni EA, Herold CJ, Brown RH, Wetzel RC, Hirshman CA, Robotham JL, and Mitzner W.** High-resolution computed tomography—physiologic correlation. *J Thorac Imaging* 8: 265–272, 1993.